

Localization of Cholesterol in Rat Cerebellum with Imaging TOF-SIMS. Effect of tissue preparation

Håkan Nygren^{a,*}, Katrin Börner^a, Per Malmberg^a, Birgit Hagenhoff^b

^a*Department of Anatomy and Cell Biology, Göteborg University, Göteborg, Sweden.*

^b*Tascon GmbH, Münster, Germany.*

* Corresponding author. *E-mail address:* hakan.nygren@anatcell.gu.se (Prof. H Nygren).

Abstract

Time-of-flight secondary-ion-mass-spectrometry (TOF-SIMS) was utilized to address the issue of cholesterol localization in rat cerebellum, a subject not previously investigated.

Rat cerebellum was prepared by three different procedures: 1. Fixation in formaldehyde, freeze-protection by sucrose, freezing in liquid nitrogen and sectioning by cryoultramicrotomy and drying at room temperature, or, 2. Freezing in liquid nitrogen, cryostat sectioning at -40°C and drying at room temperature, or, 3. High-pressure freezing, freeze fracturing and freeze drying.

The samples were analyzed in an imaging TOF-SIMS instrument equipped with a Bi_{1.7}⁺-source. The cholesterol signal (*m/z* 369 and 385), showed high intensity in the glial cells in white matter, and lower intensity in Purkinje cells and in nuclei of granular layer cells. Specimen treated by procedure 1 showed some signs of diffusion of cholesterol in the tissue. Specimen treated by procedure 2 showed freeze-damage of the cells. Specimen treated by procedure 3 showed distinct localization of cholesterol in well preserved tissue. Thus, high pressure freezing and freeze fracturing was used for further characterization of the distribution of cholesterol in rat cerebellum.

Key words: Cryofixation, imaging mass spectrometry, High pressure freezing, Bi – LMIG

1. Introduction

The cerebellum is the integrative organ for coordination and fine synchronization of body movements and for regulation of muscle tone. The organ is divided into a cortex, containing nerve cells and glial cells and a medulla containing nerve fibers and glial cells. The cerebellar cortex consists of three layers: The molecular, Purkinje cell and granular layers, all containing nerve cells interconnected by nerve fibers and synapses [1]. The function of nervous tissue is profoundly related to the function of its synapses. Recently, data have been presented showing that cultured neurons require glia-derived cholesterol to form numerous and efficient synapses [2]. The localization of cholesterol in nervous tissue is thus of interest, and has not previously been demonstrated in the cerebellum. The localization of cholesterol in cells and tissues has been thoroughly studied with specific probes like filipin [3] or perfringolysin O-toxin [4]. In synapses of the electric organ of *Torpedo marmorata* filipin-cholesterol complexes were found in patches on the presynaptic membrane and on the bottom part of the postsynaptic invaginations [5]. In chick retina, the synaptic vesicle fusion zone of ribbon junctions contain large numbers of filipin-sterol complexes together with the nonsynaptic membrane of photoreceptor terminals [6]. The results from studies using filipin for the localization of cholesterol have been criticized due to lack of penetration and low reaction rate constant of complex formation [7].

Here, we introduce bioimaging TOF-SIMS as a means to localize cholesterol. Time-of-flight secondary ion mass spectrometry (TOF-SIMS) is a technique allowing identification and localization of unknown molecules at sample surfaces [8]. It has several advantages over alternative methods e.g. its sensitivity to all elements, detection of all isotopes, excellent spatial resolution (< 300 nm), and simultaneous imaging of the surface distribution of detected elements and molecules [9]. Given this new opportunity of localizing cholesterol in rat cerebellum, we have investigated the effect of tissue preparation.

2. Materials and Methods

2.1 Animals and tissue preparation

Procedure 1: Male Sprague-Dawley rats (300g) were sacrificed by terminal anesthesia and perfusion with 4% formaldehyde in 0.05M cacodylate buffer. The samples were fixed for 15 hours and infiltrated with 2.3M sucrose for 24 hours to achieve cryoprotection.

Cryoultramicrotome sections were prepared as described by Tokuyasu [10]. Briefly, the tissue samples were mounted on specimen pins, vitrified by plunge-freezing into liquid propane at -170°C and stored in liquid nitrogen until they were sectioned. With cryoprotection, samples will remain vitrified at higher temperatures and can be cryosectioned at -80°C resulting in good sections with few cracks. Ultrathin cryosections ($0.4\ \mu\text{m}$) were cut with a Reichert Ultracut E equipped with an FC 4E cryounit. The sections were picked from the knife surface with a wire loop containing a small drop of 2.3 M sucrose solution. The sections, thawed on the drop, were then applied to cover glasses, rinsed with a drop of saline which was finally removed by a rapid rinse in distilled water. Thus, salt precipitation was avoided at the surface of the tissue section during air drying. The dry samples were stored in a desiccator before analysis. For biological samples, like tissue sections, a plane surface is important in order to avoid topographic effects during the analysis. Cryoultramicrotomy yields plane sections over limited areas, but knife scratches and rifts are frequent artefacts that may disturb the formation of an even metal film. Another source of artefacts is the compression of sections during cutting [11]. However, this problem is partly overcome by thawing the sections before mounting on glass.

Procedure 2: The rats were deeply anaesthetized with Isofluran Baxter (Baxter Medical AB, Kista, Sweden) and sacrificed under anaesthesia. To access the rat cerebellum, the skin was removed and the cranium opened carefully. With a scalpel, the cerebellum was dissected by transection of the connections with pons and medulla oblongata. The cerebellar hemispheres were separated from the vermis and cut in smaller tissue blocks of about 3-4 mm in diameter which were directly frozen in liquid nitrogen. The frozen tissue was cut with a Leica cryostat at -40°C in slices of $8\ \mu\text{m}$ thickness. The slices were placed on an object slide and dried at room temperature. Until measurement with TOF-SIMS, the samples were kept dry in a desiccator.

Procedure 3: With a scalpel, the cerebellum was dissected by transection of the connections with pons and medulla oblongata. All further steps were carried out under cold conditions, keeping the tissue in ice-cold phosphate buffered saline, 0.05 M phosphate buffer pH 7.4 (PBS). Directly after tissue preparation, the dura mater was removed and the cerebellum hemispheres were dissected under a stereomicroscope. The hemispheres were glued on a vibratome sample holder with Roti@coll tissue glue and immediately embedded in 3 % Agar noble when it was almost hardened. For vibratome cutting (Leica, VT1000S), we filled the ice-cooled chamber with cold PBS and mounted the sample holder with the embedded tissue in the instrument. At first, a slice of $900\ \mu\text{m}$ thickness was cut with the vibratome, which was discarded. Then the tissue was cut in $300\text{-}350\ \mu\text{m}$ thick slices, which were used for high-pressure freezing.

High-pressure freezing of cerebellum samples

This step was easy to accomplish, using the EMPACT (Leica, Vienna). As described in detail by [12], high pressure freezing was performed at 2000 bar and -196°C with liquid nitrogen. For our experiments, we used the freeze-fracture equipment available for this system. This included a punch with a punch rubber to prepare the tissue and special designed freeze fracture holder, composed of a carrier with a copper ring on top, which contained the sample. As soon as a vibratome section was cut, smaller tissue samples of about 1.2 mm in diameter were punched out. Regions for punching were chosen from the cortex or outer regions of the white matter in the cerebellum arbor vitae. The outermost cell layers of the slice were excluded to avoid possible embedding or chemical artefacts

from this region. The punched tissue was placed on the freeze-fracture carrier under a stereomicroscope. Excess PBS was removed with a filter paper and that followed the copper ring was put on top of the loaded carrier. With help of the loading station, this sandwich-like arrangement was placed into the loading device, which in turn was inserted into the instrument. After cryofixation, the carriers were collected in the liquid nitrogen bath of the EMPACT.

Freeze fracturing and freeze drying of the frozen samples

The samples were quickly transferred on a pre-cooled copper block in liquid nitrogen. With help of a pair of forceps, the copper ring was removed from the carrier to lay open a fractured surface. Afterwards, the copper block was transferred together with the samples into a vacuum chamber and freeze-dried over night at 10^{-3} mbar [13]. The samples were kept in a desiccator under vacuum until TOF-SIMS measurements.

2.2 TOF-SIMS analysis

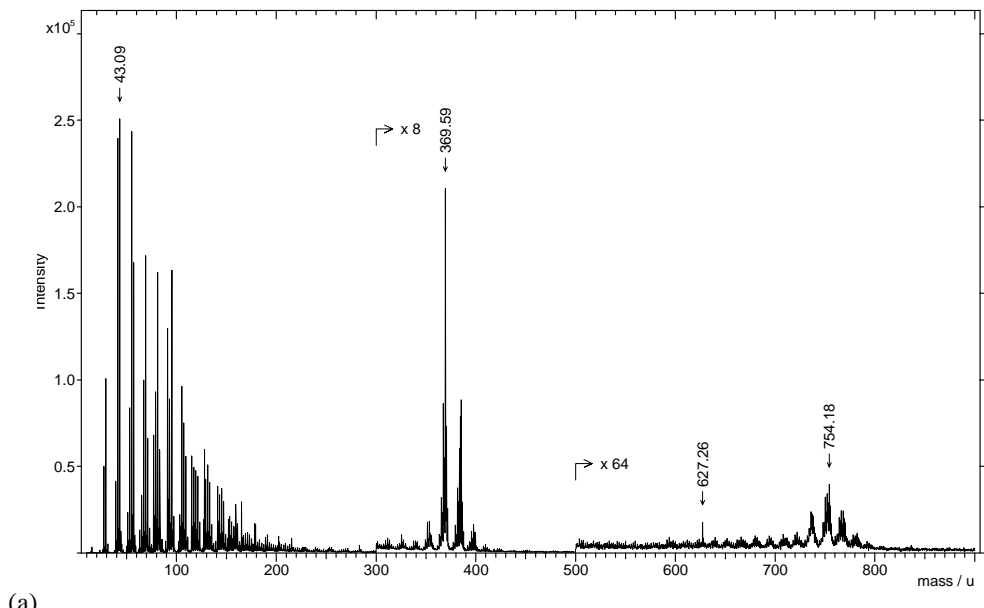
The tissue sections were analyzed with a TOF-SIMS mass spectrometer. Measurements were performed using both, an IONTOF TOF-SIMS IV and an IONTOF TOF-SIMS 5 instrument. Both instruments were equipped with a Bi liquid metal ion gun (Bi LMIG). First, surface spectra were taken from an area of $100 \times 100 \mu\text{m}^2$ in order to identify the species present at the respective surfaces. Here, the bunched mode was used (high mass resolution, $3 \mu\text{m}$ lateral resolution). Both Bi_1^+ and Bi_3^+ primary ions were applied with target currents of 0.4 and 0.15 pA, respectively. The high mass resolution and high mass accuracy allowed to assign sum formulas to peaks even in the high mass range. Subsequently, mass resolved secondary ion images were acquired in burst alignment mode using Bi_3^+ (nominal mass resolution, lateral resolution 300 nm). The target current was 0.1 pA. Fields of view ranged from $60 \times 60 \mu\text{m}^2$ to $500 \times 500 \mu\text{m}^2$ and the pixel density was 256×256 . The field of view is given in figure legends.

3. Results

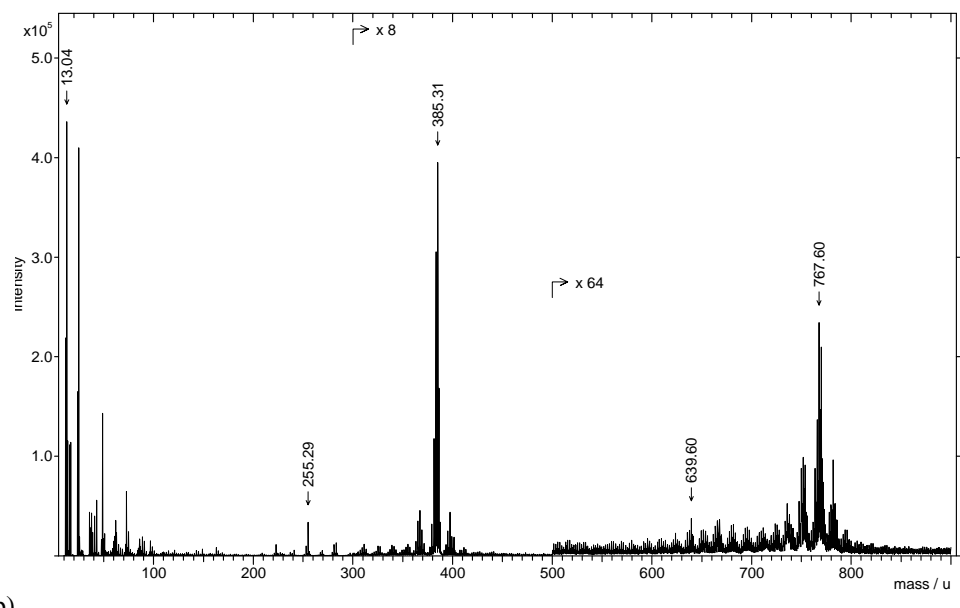
Positive and negative mode TOF-SIMS reference mass spectra for cholesterol are shown in Figure 1. Significant peaks are seen at m/z 369 and 385, representing cholesterol. These peaks were used for imaging the localization of cholesterol in the tissue sections.

Selected ion images of freeze protected rat cerebellum sections are shown in Figure 2. The total ion image (Fig. 2a) shows the molecular layer (M), the Purkinje cell layer (P) and the granular layer (G) of the cerebellum. The emission of total ions is higher in the granular layer and in the Purkinje cell than in the molecular layer.

The localization of the cholesterol signal (Fig. 2b) shows a high intensity in structures that, based on the localization and size may represent the nuclei of cells in the inner parts of the granular layer. Lower specific ion intensity is seen as dots in Purkinje cells and as patches in the granular layer (G). In the molecular layer (M), an even lower intensity of the cholesterol signal was seen localized in small dots.

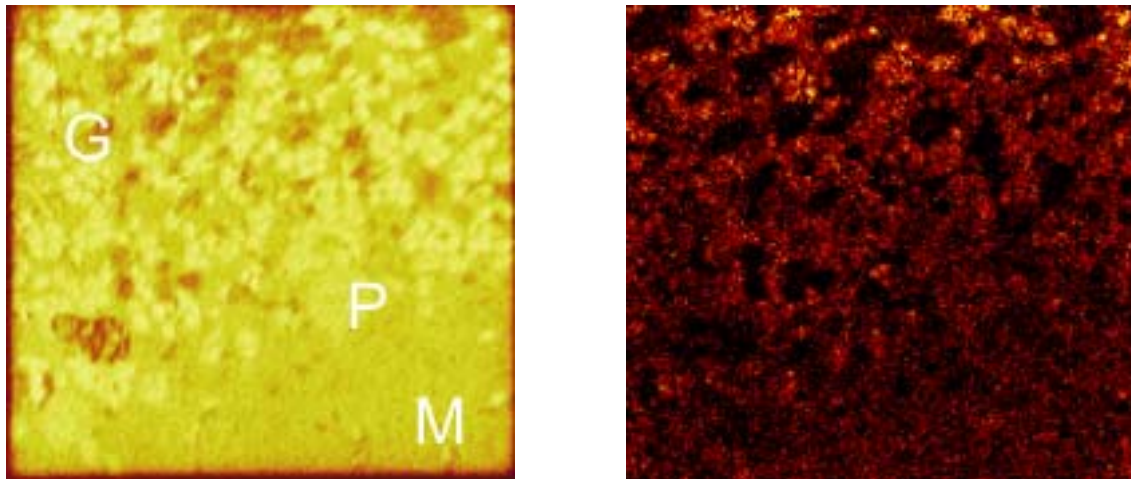


(a)



(b)

Fig. 1. Positive (a) and negative (b) TOF-SIMS mass spectra from Cholesterol analysed with an Ion-ToF, ToF-SIMS IV instrument, equipped with a Bi³⁺ liquid metal ion gun. Cholesterol (Sigma Chem Co) was dissolved in chloroform:methanol:water 60:30:4.5 (10 μ M) and placed on a clean glass surface.

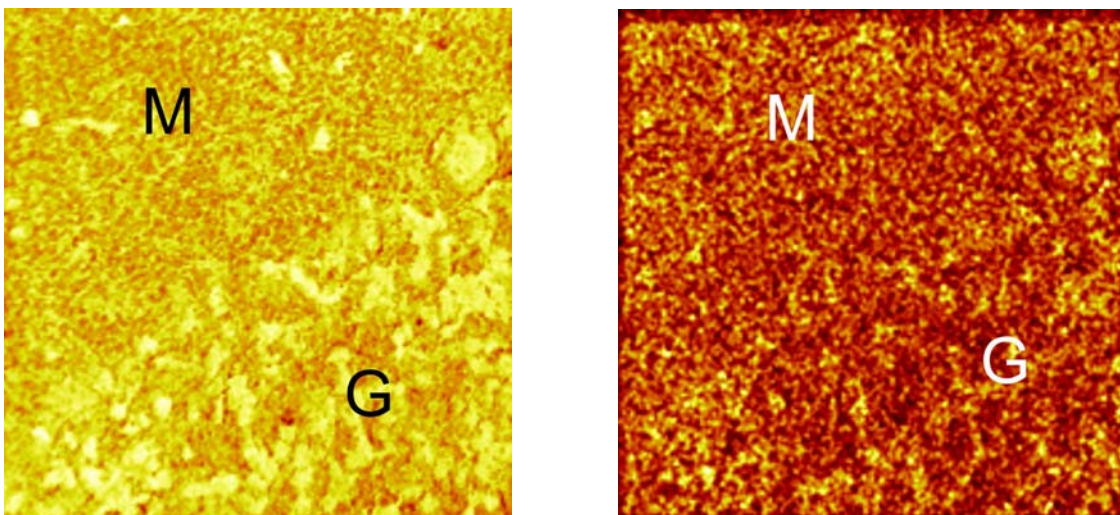


(a)

(b)

Fig. 2. Selected ion images of rat cerebellum showing the distribution of positively charged secondary ions. The specimen was prepared according to procedure 1 (M&M). Positive TOF-SIMS images of total ion counts (Fig. 2a) and cholesterol, at m/z 369 and 385, (Fig. 2b). Image sizes = $174 \mu\text{m} \times 174 \mu\text{m}$.

Figure 3 shows the distribution of negatively charged secondary ions (total ion image; Fig. 3a) and the cholesterol distribution on a cryostat sectioned cerebellum slice (Figure 3b). The total ion image (3a) gives an overview of intensities of specific regions, showing here the molecular (M) and granular layers (G) of rat cerebellum. Regions with higher ion intensities were seen in the granular layer and some few spots in the molecular layer. The cholesterol image (3b), composed of peaks at m/z 369 and 385, shows a similar distribution, but with low ion intensities in low contrast of the image. The cholesterol can be seen localized as patches in the granular layer and as a few dots in the molecular layer. The cryostat sections does not reveal any detailed localization of cholesterol at specific cells.



(a)

(b)

Fig. 3. Selected ion images of rat cerebellum showing the distribution of negatively charged secondary ions. The specimen was prepared according to procedure 2 (M&M). Negative TOF-SIMS images of total ion counts (Fig. 3a) and cholesterol, at m/z 369 added with m/z 385, (Fig. 3b). Field of view (3a) $443 \times 443 \mu\text{m}^2$ and (3b) $191 \times 191 \mu\text{m}^2$. The transition of the granular layer (G) to the molecular layer (M) is indicated.

Figure 4 shows the same area analyzed for positive secondary ions for (4a) total ion counts and (4b) the composite image of the cholesterol fragments at m/z 369 and 385. Both images show higher secondary ion intensities in the granular and lower intensity in the molecular layer. Cholesterol is found localized in patches in the granular layer and as a few dots in the molecular layer. The tissue preparation does not allow any detailed localization of cholesterol at specific cells.

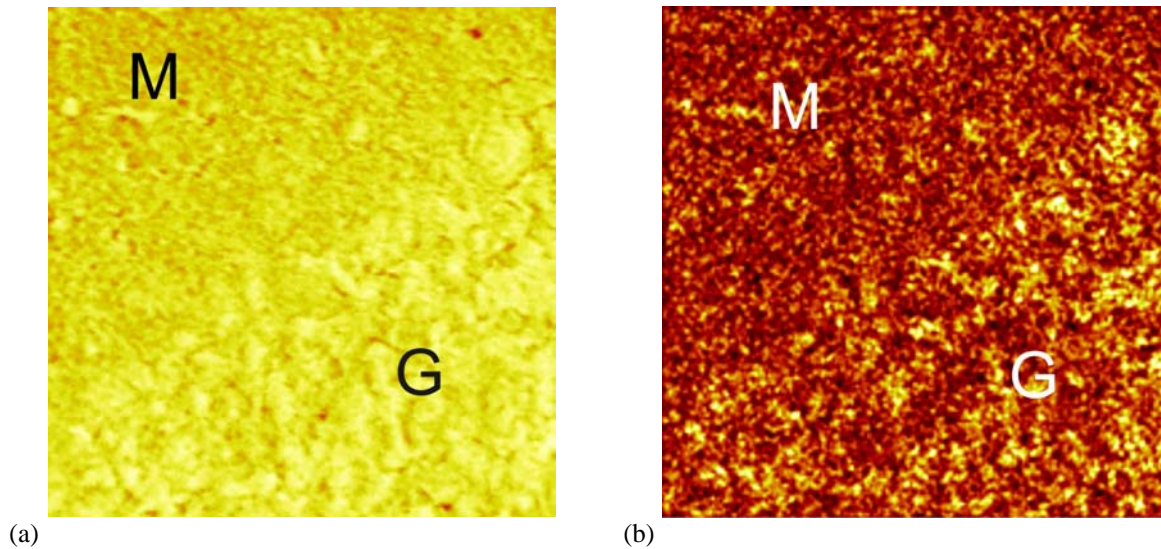
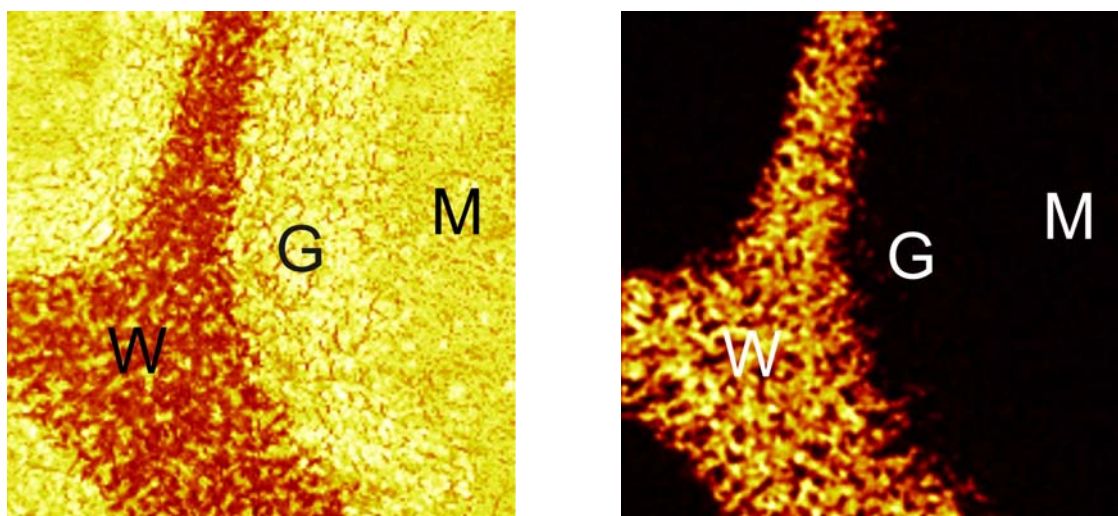


Fig. 4. Selected ion images of rat cerebellum showing the distribution of positively charged secondary ions. The specimen was prepared according to procedure 2 (M&M). Positive TOF-SIMS images of total ion counts (Fig. 4a) and cholesterol, at m/z 368 added with m/z 369 and m/z 385, (Fig 3b) in cerebellum sample. Field of view (4a) $443 \times 443 \mu\text{m}^2$ and (4b) $191 \times 191 \mu\text{m}^2$. The transition of the granular layer (G) to the molecular layer (M) is indicated.

Figure 5 shows selected ion images of a cryostat section over all cerebellar layers in a bigger field of view of $443 \times 443 \mu\text{m}^2$. The image of total negatively charged secondary ions (5a) shows different intensities of recorded secondary ions in the cortical layers, with a higher intensity in the granular layer. A lower intensity of secondary ions is seen in the white matter. The distribution of cholesterol in a composite image of m/z 369 and 385 is shown in Figure 5b. The cholesterol signal is high in the white matter, with a spotlike distribution of the highest intensities. Distinct higher intensities are also seen in the inner parts of the granular layer cell (5b and c).

Selected ion images of high-pressure frozen, freeze fractured samples of rat cerebellum are shown in Figure 6. The total count of recorded positive ions is shown in Fig. 6a. A high intensity is shown in the lower left corner of the image, representing the inner granular layer and a lower intensity is seen in the upper part of the image, representing the white matter. The localization of cholesterol in freeze-fractured high pressure frozen samples is shown in Figure 6b (linear representation) and 6c (logarithmic representation). Cholesterol is seen localized in spots in the white matter and inner region of the granular layer. The narrow dynamic range of the instrument gives a false contrast to the linear image, but the presence of cholesterol in the granular layer is clearly seen in the logarithmic image.



(a)

(b)

Fig. 5. Selected ion images of rat cerebellum showing the distribution of positively charged secondary ions. The specimen was prepared according to procedure 2 (M&M). Negative TOF-SIMS images of total ion counts (Fig. 5a) and cholesterol, at m/z 369 added with m/z 385, (Fig 5b) and logarithmic presentation of the cholesterol signal (Fig. 5c). The images are taken over a section of the cortical granular (G) and molecular (M) layers and white matter (W).

Field of view (5a) $443 \times 443 \mu\text{m}^2$
and $191 \times 191 \mu\text{m}^2$ (5b).

(c)

4. Discussion

Secondary ion mass spectrometry is based on the outcome of the impact of high energy primary ions onto a target. Using traditional ion sources e.g. the gallium ion source the yield of large molecular fragments, necessary for the identification of the original molecule, seems to be limited [14]. The bismuth-gold cluster ion source, used in the present study, significantly improves the yield of large molecular fragments and several fragments can be identified as identical to those found with other mass spectrometry methods. The peaks at m/z 369 and 385 have been demonstrated with chemical ionization MS [15].

The topography of the sample may affect the intensity of the sputtering of secondary ions. Samples prepared by cryoultramicrotomy (procedure 1) are plane [16] still, the intensity of the total ion emission differs between the layers of cerebral cortex. Cryostat sections and freeze fractured surfaces may not be completely plane and topographical effects are more likely to occur when analysing these specimen by TOF-SIMS. However, the distribution of total secondary ions is similar between samples prepared by all three methods and we thus conclude that the heterogeneous distribution of total ions and cholesterol seen in this study represents a true heterogeneity in the localization of the emitted ions. We may then consider if the localization recorded is the native one.

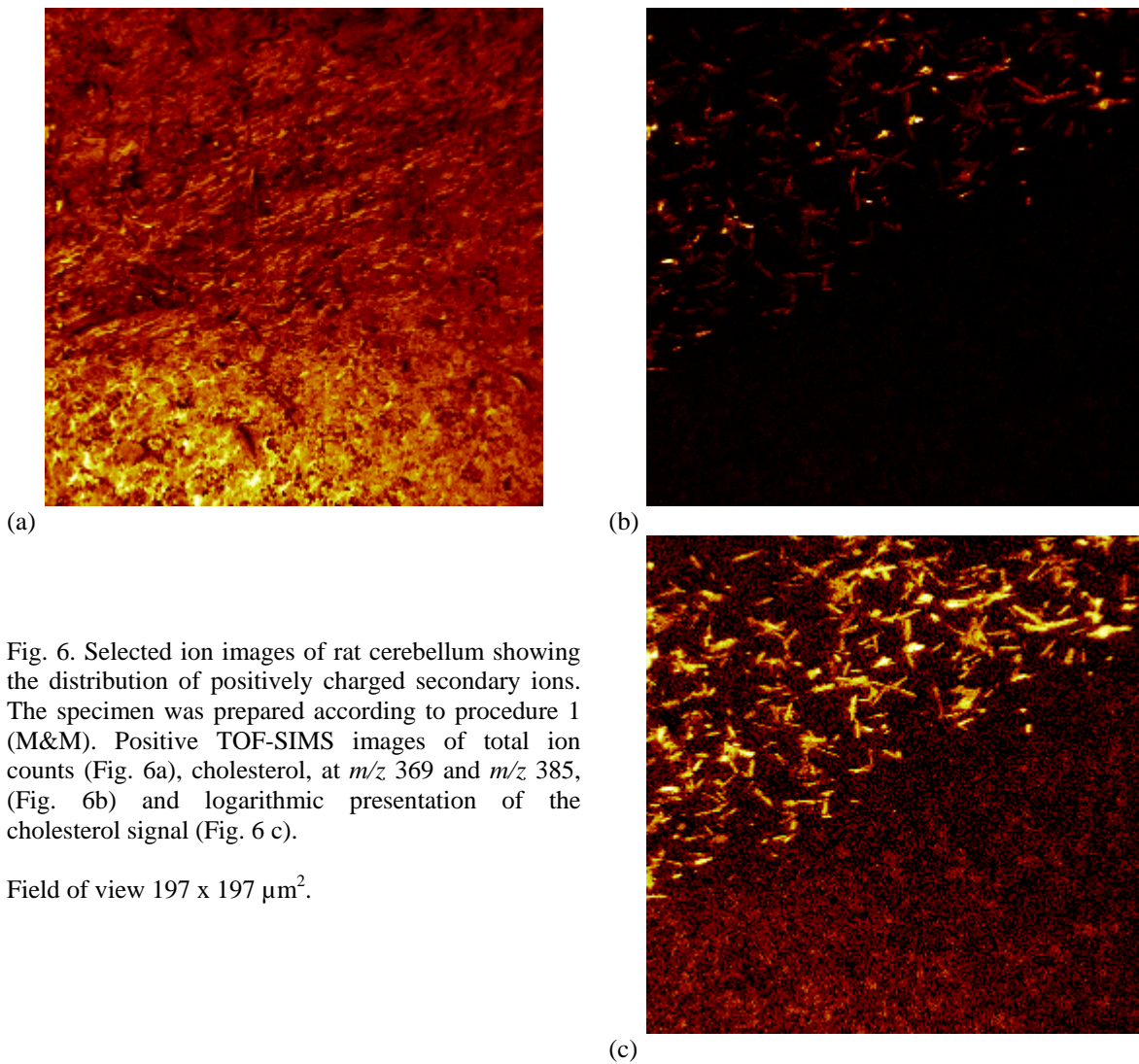


Fig. 6. Selected ion images of rat cerebellum showing the distribution of positively charged secondary ions. The specimen was prepared according to procedure 1 (M&M). Positive TOF-SIMS images of total ion counts (Fig. 6a), cholesterol, at m/z 369 and m/z 385, (Fig. 6b) and logarithmic presentation of the cholesterol signal (Fig. 6 c).

Field of view $197 \times 197 \mu\text{m}^2$.

Cholesterol is not fixed by aldehydes, and the possible extraction of cholesterol during tissue preparation has to be noted [7,17]. Yet, despite the fact that cholesterol is not immobilized by common fixation techniques, cholesterol losses during aldehyde preparation tissue types is minimal [18]. The heterogeneous cholesterol distribution depending on different sample preparation techniques indicates that relocation artefacts mostly affect plasma membranes and not intracellular membranes [17]. The recorded localization of cholesterol in cell nuclei in the granular layer may thus be due to selective preservation of an intracellular pool of cholesterol. When compared with fast freezing methods, the localization of cholesterol seems more fuzzy in the freeze-protected samples, suggesting possible diffusion artefacts due to inadequate fixation of cholesterol during freeze protection.

Samples sectioned with a Cryostat microtome showed good morphology at overview magnifications, but the tissue was fragmented at higher magnification, and it was not possible to identify structures at the cellular level. This technique has been used in almost all studies on analysis of tissues with imaging TOF-SIMS, and it is not adequate for cellular or subcellular localization of cell constituents.

The advantage of procedures 1 and 2 is the use of reference sections allowing orientation of the analyzed area in a routine histological image of an organ.

The ultimate aim of tissue fixation is to preserve all elements of the tissue at their original location. The only way to reach that aim, described so far, is high-pressure freezing (HPF) of small tissue

pieces, preserving even the water in its amorphous, vitrified state [12,19]. Freeze-drying of the specimen before analysis, according to a procedure described by Warley and Skepper [13], was introduced to avoid the presence of water in the spectra.

High pressure frozen, freeze fractured samples showed good morphological preservation at all levels of resolution allowing cellular and subcellular localization of cholesterol. The highest levels of cholesterol signal were found in white matter in structures which morphologically resemble glial cells, probably representing oligodendrocytes.

Cholesterol is a versatile molecule known as an essential membrane component and a precursor for steroid hormones. New facets of cholesterol function are continuously defined, e.g. an active role in cell signalling and membrane structure formation and function [20,21] as a messenger between astrocytes and neurons in the regulation of synapse formation [22].

In this work, cholesterol can be seen localized primarily in the white matter oligodendrocytes and in myelin, but also in the Purkinje cells and in the nuclei of cells of the granular layer. The localization of cholesterol in white matter probably represents synthesis of cholesterol which is a major component of myelin. The cholesterol content of the Purkinje cells is probable due to the fact that Purkinje cells are a major site of neurosteroidogenesis in the brain [23], and a nuclear localization of cholesterol, as seen in the granule cells, has been reported in cells with an active uptake of cholesterol [24].

Acknowledgement: The study was supported by the National Research Council (VR, NT) and by the SWEGENE project.

References

- [1] Heck, D. and Sultan, F. (2002) *Hum Mov Sci* 21, 411-21.
- [2] Mauch, D.H., Nagler, K., Schumacher, S., Goritz, C., Muller, E.C., Otto, A. and Pfrieder, F.W. (2001) *Science* 294, 1354-7.
- [3] Severs, N.J. and Robenek, H. (1983) *Biochim Biophys Acta* 737, 373-408.
- [4] Fujimoto, T., Hayashi, M., Iwamoto, M. and Ohno-Iwashita, Y. (1997) *J Histochem Cytochem* 45, 1197-205.
- [5] Perrelet, A., Garcia-Segura, L.M., Singh, A. and Orgi, L. (1982) *Proc Natl Acad Sci U S A* 79, 2598-602.
- [6] Cooper, N.G. and McLaughlin, B.J. (1984) *J Comp Neurol* 230, 437-43.
- [7] Miller, R.G. (1984) *Cell Biol Int Rep* 8, 519-35.
- [8] Benninghoven, A. (1994) *Surface Science* 300, 246-260.
- [9] Chabala, J.M., Soni, K.K., Gavrillov, K. and Levi-Setti, R. (1995) *Int J Mass Spectrom Ion Processes* 143, 191-212.
- [10] Tokuyasu, K.T. (1986) *J Microsc* 143 (Pt 2), 139-49.
- [11] Al-Amoudi, A., Dubochet, J., Gnaegi, H., Luthi, W. and Studer, D. (2003) *J Microsc* 212, 26-33.
- [12] Studer, D., Graber, W., Al-Amoudi, A. and Eggli, P. (2001) *J Microsc* 203, 285-94.
- [13] Warley, A. and Skepper, J.N. (2000) *J Microsc* 198 (Pt 2), 116-23.
- [14] Todd, P.J., McMahon, J.M., Short, R.T. and McCandlish, C.A. (1997) *Analytical Chemistry* 69, A529-A535.
- [15] Lin, Y.Y. (1980) *Lipids* 15, 756-63.
- [16] Nygren, H., Johansson, B.R. and Malmberg, P. (2004) *Microsc Res Tech* 65, 282-6.
- [17] Möbius, W. et al. (2002) *J Histochem Cytochem* 50, 43-55.
- [18] Mitchell, C.D. (1969) *J Cell Biol* 40, 869-72.
- [19] Al-Amoudi, A. et al. (2004) *Embo J* 23, 3583-8.
- [20] Simons, K. and Ikonen, E. (1997) *Nature* 387, 569-72.
- [21] Ikonen, E. and Parton, R.G. (2000) *Traffic* 1, 212-7.
- [22] Pfrieder, F.W. (2003) *Biochim Biophys Acta* 1610, 271-80.
- [23] Tsutsui, K., Sakamoto, H. and Ukena, K. (2003) *Cerebellum* 2, 215-22.
- [24] Bjorkhem, I. and Meaney, S. (2004) *Arterioscler Thromb Vasc Biol* 24, 806-15.